Particle Accelerators, 1997, Vol. 56, pp. 127–145
Reprints available directly from the publisher
Photocopying permitted by license only

ELECTRON BUNCH COMPRESSION DUE TO RF FORCES IN AN RF PHOTOINJECTOR FOR SMALL RF LAUNCH PHASES

BRUCE E. CARLSTEN and DINH C. NGUYEN

Los Alamos National Laboratory, Los Alamos, NM 87545, USA

(Received 5 March 1996; in final form 7 August 1996)

The compression of a short, low-charge electron bunch in the first cell of an rf photoinjector is calculated for start phases of the electron bunch well before the peak of the accelerating electric field. This bunch compression results from a larger rf acceleration of the rear of the bunch than that of the front of the bunch due to the sinusoidal time dependence of the rf fields. The calculation in this paper shows that compressions of 50%, and more, of the initial bunch length are possible for early start phases, if the space-charge forces are negligible. Both a very accurate integral representation and a fairly accurate approximate formula for the compression are presented, which are valid for start phases from zero to about $\pi/2$ radians, and for accelerating gradients ranging from those in on-going experiments to gradients several times larger.

Keywords: Beam transport; particle dynamics; radio-frequency devices.

1 INTRODUCTION

RF photoinjectors have been used for the generation of short-length, high-brightness electron bunches.[1–6] In a photoinjector, electrons are emitted from a cathode embedded in an rf cavity when the cathode is illuminated by the light from an external laser (with a duration from a few to tens of picoseconds). The accelerating electric field in the rf cavity quickly accelerates the electron bunch to relativistic energies before the space-charge forces have enough time to degrade the transverse emittance of the bunch. After the bunch leaves the first cavity (typically at a relativistic mass factor of two or more), it encounters additional cavities phased in a manner to continue the acceleration. The effect of the longitudinal space-charge force is minimized by the rapid acceleration, and the longitudinal bunch distribution can be customized by

adjusting the temporal laser pulse profile. As a result, photoinjectors are often used for driving free-electron lasers where high current and low emittance is very desirable, and have been proposed for electron beam injectors for high-average current machines where interception of the electrons along the beam pipe must be minimized. The operating frequency of the photoinjectors in the experiments referenced above has ranged from 144 MHz to 17 GHz.

The electron emission from the cathode surface is prompt with respect to the laser light (for the proper cathode material), and thus the initial longitudinal distribution is determined by the temporal characteristic of the laser. This feature has led to the proposal of using a very short laser pulse length to generate a very short electron bunch (on the order of 100 fs, or less).[7–9]

It has been recognized that if the trailing end of the electron bunch is emitted at an rf phase leading to a larger accelerating gradient than that of the front, the bunch will be compressed by the difference of the rf forces.[9–13] Counteracting this compression is the longitudinal space-charge force which tends to expand the bunch. Both of these features primarily occur very close to the cathode, before the beam becomes relativistic. These features have been measured with a streak camera in an early experiment[3], and for moderate charges (about 5 nC) and low gradients (25 MV at 1.3 GHz), the effects are about equal. However, for low charges (0.1–1 nC), the rf compression dominates, and the overall compression can be quite large; this has been demonstrated in a recent experiment.[14]

Because the rf compression is based on the relative difference of the accelerating forces between the front and back of the electron bunch, the compression can be increased by timing the laser so that the light reaches the cathode early in the rf cycle, well before the accelerating field is peaked. Using the usual convention, we will assume that the electric field vanishes at a phase of zero degrees and is at a maximum at a phase of 90 degrees. Because of the transcendental nature of the equations governing the motion of the electron bunch, exact analytic calculations of the rf compression are not possible, and the only available approximate treatment of the rf compression[9,15] breaks down for cathode start phases significantly less than 90 degrees, where the compression becomes large.

In this paper, we will derive a very accurate integral formula for the rf compression in the first rf cavity of a photoinjector of a short electron bunch with negligible charge. An even simpler expression containing no integrals and still valid over a broad range of start phases and accelerating

gradients will be presented. This will lead to an expression for the final bunch length in terms of the initial bunch length, the accelerating gradient, and the start phase of the center of the electron bunch. The lowest-order effect of the longitudinal space-charge force can be added into this expression, if desired, by using a formula given in Reference 9. The following analysis will be one-dimensional, but this will not limit the results significantly because near the cathode the beam is much wider than it is long (and thus is essentially one-dimensional). Three-dimensional effects have been considered in Reference 9 and shown to be negligible for most cases of interest. The drive laser length will additionally be considered sufficiently short so that the final electron bunch length depends only linearly on it.

2 AXIAL MOTION IN THE FIRST CAVITY OF AN RF PHOTOINJECTOR

Ignoring transverse effects, the equation that governs the axial evolution of a particle that leaves the cathode at a phase ϕ_o is the one-dimensional Lorentz force equation

$$\frac{d^2}{dt^2}z = \frac{e}{\gamma^3 m}E_z(z,t) \tag{1}$$

(the apparent extra γ^2 term in the denominator arises from the time derivative of the relativistic mass factor γ), and where $E_z(z,t)$ is the axial electric field in the first rf cavity. The equivalent expression for the evolution of the relativistic mass factor is

$$\frac{d\gamma}{dz} = \frac{e}{mc^2}E_z(z,t). \tag{2}$$

The boundary conditions used with Equations (1) and (2) are that $z = 0$, $dz/dt = 0$, and $\gamma = 1$ all at $t = 0$. If the first cell is designed to support only the lowest-order space harmonic (and thus is exactly one-half free-space rf wavelength long), the axial electric is given by

$$E_z(z,t) = E_o \cos(kz)\sin(\omega t + \phi_o) \tag{3}$$

where now E_o is some constant, $\omega/2\pi$ is the rf frequency, and $k = \omega/c$. Equations (1)–(3) represent the commonly accepted description of the axial evolution of particles in a photoinjector (see for example References 9, 11, and 15). The shapes of the first cavity of some rf photoinjectors deviate slightly from supporting just the first space harmonic, however this will not be important as we will see later. In principle, these equations can be solved to find the axial position z as a function of both time and initial phase ϕ_o; once z is known, it can be differentiated with respect to ϕ_o and the bunch lengthening or contraction from the rf forces can be determined. In practice, this set of equations can not be solved except by numerical means and a simple expression for the bunch lengthening must be found empirically, or by using approximations in Equations (1)–(3).

Note that Equations (1)–(3) can be written in the purely normalized manner

$$\frac{d^2}{d\tau^2}\zeta = \frac{2\alpha}{\gamma^3}\cos(\zeta)\sin(\tau + \phi_o) \tag{4}$$

and

$$\frac{d\gamma}{d\zeta} = 2\alpha\cos(\zeta)\sin(\tau + \phi_o), \tag{5}$$

where $\tau = \omega t$ is a normalized time, $\zeta = \omega z/c$ is a normalized axial position, and the normalized accelerating gradient is given by $\alpha = eE_o/2\omega mc$. A normalized gradient of unity leads to an actual peak accelerating gradient at the cathode of 27.8 MV/m at 1.3 GHz, 61.2 MV/m at 2.856 GHz, and 364.6 MV/m at 17 GHz. Most current photoinjectors operate in the region of $\alpha \sim \frac{1}{2} - \frac{3}{2}$. The advantage of writing the axial motion in the normalized forms is that it becomes clear that the solution only depends on α, the initial phase ϕ_0, and the final normalized time τ_{end} at the end of the photoinjector cavity. Thus the actual photoinjector frequency only enters in the normalized gradient α, and for equal α and ϕ_o, photoinjectors at different frequencies will lead to the exact same ratio of the final, compressed bunch length to the initial, uncompressed bunch length. In this paper, we will consider a compression ratio defined to be the amount of compression over the initial bunch length; this way the results are independent of operating frequency. Note that this is a somewhat different definition of compression ratio than used elsewhere, and that a compression ratio of zero means no compression and of unity means compression to an infinitely short bunch. We will use this definition in order

to minimize algebraic manipulations that do not lead to additional physical insights.

Also note that several photoinjectors do not satisfy the requirements leading to Equation (3); the first cavity of the photoinjector in Reference 3 has a recessed cathode and the first cavity of the photoinjector in Reference 4 has a first cell that is longer than one-half the free-space rf wavelength. In fact, the axial electric field in the photoinjector in the case of in Reference 3 rises slightly as one moves axially out from the cathode (if one ignores the sinusoidal time dependence), and is overall flatter than Equation (3) suggests. In addition, it is reasonable to expect that most of the bunch length expansion or contraction takes place while the beam is nonrelativistic and thus close to the cathode. This leads us to consider the case where there is no axial dependence on the axial field, and it is given by

$$E_z(z,t) = E_o \sin(\omega t + \phi_o). \tag{6}$$

With this approximation, the axial motion of a particle can be found analytically.

Starting with Equations (2) and (4) we see

$$\frac{d\gamma}{dt} = \frac{d\gamma}{dz}\frac{dz}{dt} = \frac{e}{mc} E_o \sin(\omega t + \phi_o)\beta, \tag{7}$$

where, as usual, $\beta^2 = 1 - \gamma^{-2}$. After integrating Equation (7), we find

$$\gamma = \sqrt{4\alpha^2(\cos(\phi_o) - \cos(\omega t + \phi_o))^2 + 1} \tag{8}$$

and

$$\beta = \frac{1}{c}\frac{dz}{dt} = \frac{2\alpha(\cos(\phi_o) - \cos(\omega t + \phi_o))}{\sqrt{4\alpha^2(\cos(\phi_o) - \cos(\omega t + \phi_o))^2 + 1}}, \tag{9}$$

where we are again using the normalized gradient.

Integrating a particle's velocity, we find that its position as a function of time is given by

$$z(\phi_o, t) = \int_0^t c \frac{2\alpha(\cos(\phi_o) - \cos(\omega t' + \phi_o))}{\sqrt{4\alpha^2(\cos(\phi_o) - \cos(\omega t' + \phi_o))^2 + 1}} dt', \tag{10}$$

which does not conveniently reduce. However, since we are interested in the change in the bunch length as it is accelerated, we don't need to solve Equation (10). We will assume that the drive laser length is sufficiently short so that the compression only depends on the first order compression ratio term. In that case, the bunch length change (in time) is given by $\Delta t = \Delta l/\beta c$, where the bunch length change (in distance) is

$$\Delta l = \int_0^t \frac{d(\beta c)}{d\phi_o} \Delta\phi_o dt', \tag{11}$$

the drive laser pulse length (in time) is $\Delta\phi_o/\omega$, and β is found from Equation (9). Collecting terms and differentiating, we find that the bunch length expansion (or contraction) at a time t_{end} is given by

$$\frac{\omega\Delta l}{\beta c\Delta\phi_o} = \frac{1}{\beta}\int_0^{\omega t_{\text{end}}} \frac{2\alpha(\sin(\omega t' + \phi_o) - \sin(\phi_o))}{(4\alpha^2(\cos(\phi_o) - \cos(\omega t' + \phi_o))^2 + 1)^{3/2}} d(\omega t'). \tag{12}$$

The first term in the numerator is easy to integrate analytically but the second term is awkward.

The approximate compression ratio at the end of the first cavity, given by numerically integrating Equation (12), can be compared to that found by numerically solving the motion of particles in the first photoinjector cavity, using Equations (1)–(3), and thus we can estimate the error introduced by neglecting the axial dependence of the accelerating field. In Figures 1(a), 1(b), and 1(c), we compare the first order compression ratio predicted by numerically integrating Equation (12) to that numerically found by the one-dimensional particle-pushing code CELL, for normalized gradients of 1/2, 1 and 2 (using an initial drive laser length of 0.05 radian). In these figures, the solid line is given by the solution of Equation (12) while the circles are the results from numerically solving Equations (1)–(3). In all cases, we see excellent agreement, with exceptional agreement as the gradient is increased (as one would expect because the beam becomes relativistic closer to the cathode surface at higher gradients). Thus, for practical photoinjector cases, the approximation used in Equation (6), and thus Equation (12), is valid.

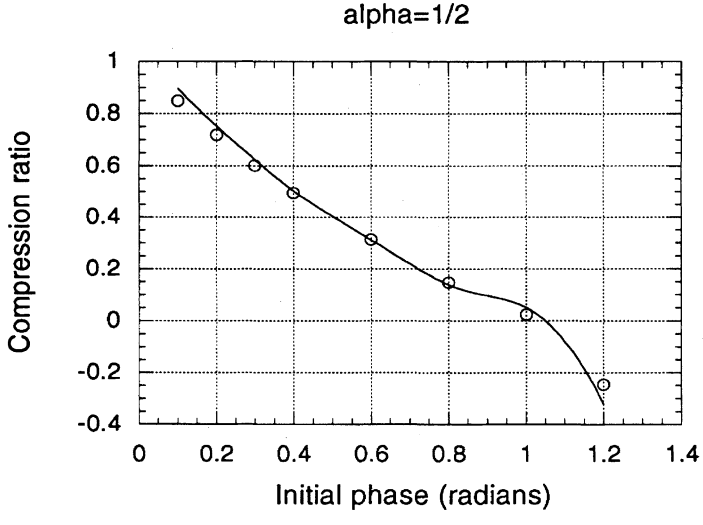

(1a)

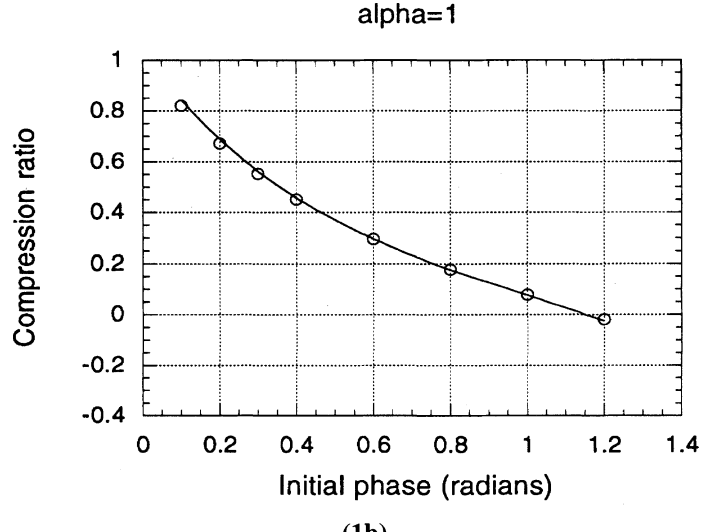

(1b)

FIGURE 1 Compression ratio versus rf start phase. The solid lines are the solutions of Equation (12) and the circles are from numerical solutions of Equations (1)–(3), (a) $\alpha = \frac{1}{2}$, (b) $\alpha = 1$, (c) $\alpha = 2$.

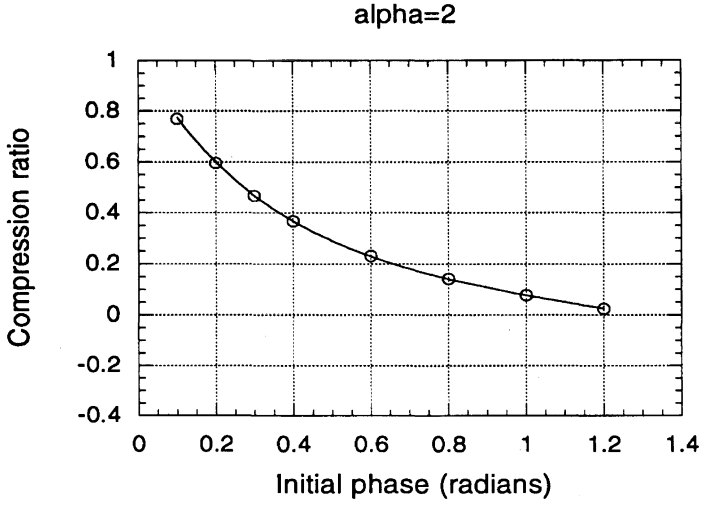

(1c)

Note that significant compression ratios are possible for relatively low start phases. The final bunch length is less than half the drive laser length for start phases of 0.25 radian or less (for sufficiently low bunch charges). Also note from the figures that the second order compression ratio term is related to the curvature of the first order compression ratio shown in Figure 1, and only becomes important for initial drive laser lengths longer than 0.1 radians.

In Figure 2 we plot the compression ratio for a start phase of 0.5 radian as a function of normalized gradient. Note that the compression ratio for this start phase peaks for a gradient of about 1/2, and slowly tapers off at higher gradients, roughly inversely proportional to the gradient. The dashed lines correspond to the solution of Equation (12) and the circles to numerical solutions of Equations (1)–(3). For gradients greater than 1/2, the cavity length was assumed to be one-half a free-space wavelength long. The line with the shorter dashes that appears for gradients less than 1/2 (and the corresponding numerical point) is for the case where the cavity length is kept at one-half a free-space wavelength. The compression ratio oscillates furiously from positive to negative for gradients below 0.15 for this case, because the bunch transit time in the cavity grows infinitely large as the gradient vanishes. The other branch with the longer dashes and circles is for

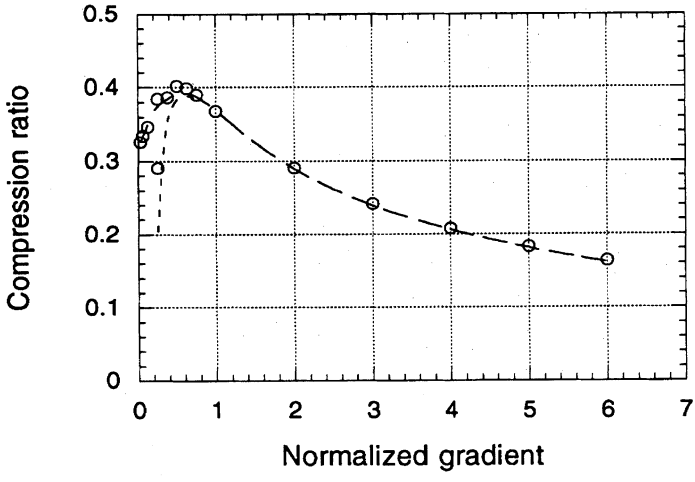

FIGURE 2 Compression ratio versus normalized gradient α for a 0.5 radian start phase. The dashed lines are the solutions of Equation (12) and the circles are from numerical solutions of Equations (1)–(3).

the case where the cavity length was adjusted so that the center of the bunch exited the cavity at a phase $\omega t + \phi_o = \pi$. For this case, the compression ratio is a relatively smooth function of the gradient, and drops to zero at very small normalized gradients.

3 HIGH GRADIENT LIMIT

We can find an approximate solution for Equation (12) in the high-gradient limit, with α large. First note the expansions

$$\sin(x + \phi_o) = \sin\phi_o + x\cos\phi_o - \frac{x^2}{2}\sin\phi_o - \frac{x^3}{6}\cos\phi_o + \ldots \qquad (13)$$

and

$$\cos(x + \phi_o) = \cos\phi_o - x\sin\phi_o - \frac{x^2}{2}\cos\phi_o + \frac{x^3}{6}\sin\phi_o + \ldots \qquad (14)$$

if x is small. For the gradients of interest, the expansions need to be kept only to second order in ωt, and Equation (12) becomes

$$\frac{\omega\Delta l}{\beta c\Delta\phi_o} = \frac{1}{\beta}\int_0^{\omega t_{\text{end}}} \frac{2\alpha\left(\omega t'\cos\phi_o - \frac{(\omega t')^2}{2}\sin\phi_o\right)}{\left(4\alpha^2\left(-\omega t'\sin\phi_o - \frac{(\omega t')^2}{2}\cos\phi_o\right)^2 + 1\right)^{3/2}} d(\omega t'). \tag{15}$$

This is also not easily integrable. However, for sufficiently high gradients, we only need to keep the linear expansion terms; this can be integrated and we find

$$\frac{\omega\Delta l}{\beta c\Delta\phi_o} = \frac{1}{2\alpha\beta}\frac{\cos\phi_o}{\sin^2\phi_o}\left(1 - \frac{1}{\sqrt{4\alpha^2(\omega t_{\text{end}})^2\sin^2\phi_o + 1}}\right), \tag{16}$$

where ωt_{end} is the normalized time at the end of the cavity. For extremely high gradients, the second term in the parentheses is very small and can be ignored. Note that Equation (16) predicts an inverse scaling with α at high gradients, seen in Figure 2.

4 LOW GRADIENT LIMIT

In this limit, the denominator of Equation (12) becomes unity, and the integration leads to

$$\frac{\omega\Delta l}{\beta c\Delta\phi_o} = \frac{2\alpha}{\beta}(1 + \cos\phi_o + (\pi - \phi_o)\sin\phi_o) \tag{17}$$

for the case the cavity length is adjusted so that $\omega t + \phi_o = \pi$ (this corresponds to the branch with the longer dashes in Figure 2). In this limit, the compression is proportional to α. This limit is of marginal use, because as demonstrated in Figure 2, it is valid only for gradients well under $\alpha = 0.1$.

5 MODERATE GRADIENT APPROXIMATION

In the range $\frac{1}{2} \leq \alpha \leq 2$, there is no exact solution to the integral in Equation (12). Unfortunately, that is the range of gradients of most existing and proposed experiments.

However, an approximate solution can be found, which leads to surprisingly accurate results. In this regime, there are several possible forms for an approximate solution, but we will pick one that maintains these physical characteristics: (1) the expression for the compression goes as $1/\alpha$ for large gradients (see Equation (16)), (2) the expression for the compression goes as α for low gradients (see Equation (17)), and (3) the expression for the compression reduces to the exact solution $\omega\Delta l/\beta c\Delta\phi_o = 4\alpha/\beta\sqrt{16\alpha^2+1}$ for $\phi_o = 0$.

At this point, consider the $[\sin(\omega t' + \phi_o) - \sin\phi_o]$ part of the numerator of Equation (12). This vanishes for $\omega t' = 0$ and for $\omega t' = \pi - 2\phi_o$ and can be represented to some level of accuracy by $\sin k\omega t'(1-\sin\phi_o)\cos\phi_o$ where $k = 1 + 2\phi_0/\pi$ [the $(1-\sin\phi_o)$ factor gives it the proper magnitude at its maximum and the $\cos(\phi_o)$ factor gives it the proper first derivative at $\omega t' = 0$]. Likewise, we can represent the sinusoidal part of the denominator by $[\cos\phi_o - \cos(\omega t' + \phi_o)] \approx (1-\cos k\omega t')(1+\cos\phi_o)/2$. With these substitutions, the integral can be done, and gives excellent agreement with the numerical solution of the integral near $\alpha = \frac{1}{2}$. As the gradient increases, the additional error introduced by the wrong curvature of the sinusoidal part of the denominator can be corrected by using in the denominator an effective normalized gradient, fitted by numerical comparisons with Equation (12). The fitted integral is then

$$\frac{\omega\Delta l}{\beta c\Delta\phi_o} = \frac{1}{\beta}\int_0^{\omega t_{\text{end}}} \frac{2\alpha\sin k\omega t'(1-\sin\phi_o)\cos\phi_o}{[\alpha^{*2}(1-\cos k\omega t')^2(1+\cos\phi_o)^2/4+1]^{3/2}}\, d(\omega t') \tag{18}$$

where the effective normalized gradient α^* is given by

$$\alpha^* = \frac{2\alpha + \frac{2\alpha^2}{3}\sin^{1/2}\phi_o}{1+\frac{\sin^{1/2}\phi_o}{6}} \tag{19}$$

After integration, this leads to

$$\frac{\omega\Delta l}{\beta c\Delta\phi_o} = \frac{1}{\beta\sqrt{\alpha^{*2}(1+\cos\phi_o)^2+1)}}\,\frac{4\alpha(1-\sin\phi_o)\cos\phi_o}{1+2\phi_o/\pi} \tag{20}$$

for the first order compression ratio at the end of the first cavity. As desired, this expression reduces properly in both the high and low gradient limits, and for $\alpha_o = 0$.

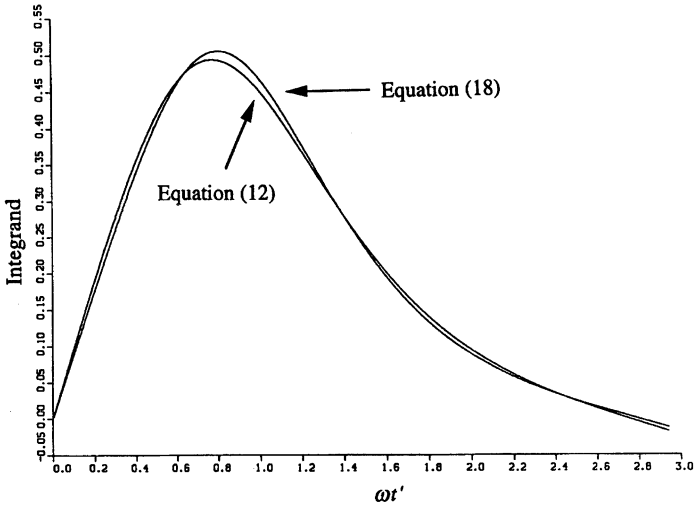

(3a)

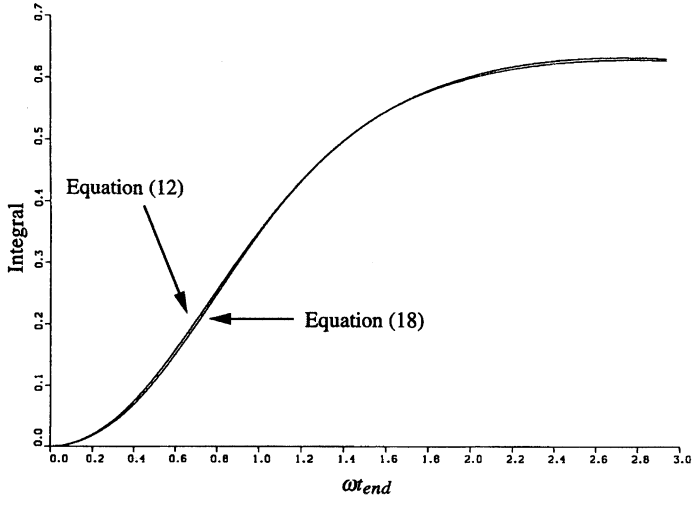

(3b)

FIGURE 3 Comparison of Equations (12) and (18) for $\alpha = \frac{1}{2}$ and $\phi_o = 0.2$. (a) Comparison of the integrands as functions of $\omega t'$. (b) Comparison of the integrals as functions of t_{end}.

The integrands in Equations (12) and (18) can be compared as functions of $\omega t'$ for a relatively low gradient ($\alpha = \frac{1}{2}$) and a relatively low start phase ($\phi_o = 0.2$), which is shown in Figure 3(a). The integrands are indeed very similar. The integrals can also be compared as functions of t_{end}, shown in Figure 3(b), and show excellent agreement.

We expect that the approximate form of the sinusoidals begins to fail at high gradients and large rf start phases. In Figure 4(a) we compare the integrands as functions of $\omega t'$ for a case where $\alpha = 2$ and the start phase is 0.6 radian. The integrands are somewhat offset in this case, from the different curvatures in the denominator. However, a comparison of the integrals versus t_{end}, shown in Figure 4(b), again shows fine agreement.

In Figure 5(a), 5(b), and 5(c), we plot the solution of the fitted integral (Equation (20)) and the numerical integration of the integral in Equation (12), for gradients of $\alpha = \frac{1}{2}, \alpha = 1$, and $\alpha = 2$, respectively. In these figures, the solid lines are from the numerically integrated solutions of Equation (12) and the circles are from the solutions of Equation (20). Over this range, the fitted solution agrees well with the approximate solution (Equation (12)) and thus the actual compression ratio from direct numerical solution of Equations (1)–(3). This approximate solution predicts the compression correctly to within an error of 2.5% for initial phases of $\pi/2$ or less up to a normalized gradient α of 5, well beyond the level of present or proposed experiments. Note that for ϕ_o very close to zero, the rf compression ratio approaches unity (infinitely thin final bunch length), in agreement with the exact solution to the integral in Equation (12) (which can be seen using Equation (9)). Additional compression is possible in subsequent rf cavities or drifts.[14] For most cases of interest, however, the majority of the compression occurs in the first cavity, and is given by Equation (20).

6 COMPARISON WITH PARMELA

In order to demonstrate the usefulness of Equation (20), we show in Figure 6 a comparison of compression ratios calculated by the accelerator simulation code PARMELA[16] and by Equation (20). The Brookhaven National Laboratory S-band photoinjector[5] was used for this comparison, operating at an average accelerating gradient of 75 MV/m and a peak field on the cathode of 112.5 MV/m, or a normalized gradient of 1.84 at a frequency of 2.856 GHz. (Using Equation (3) to describe the axial field distribution,

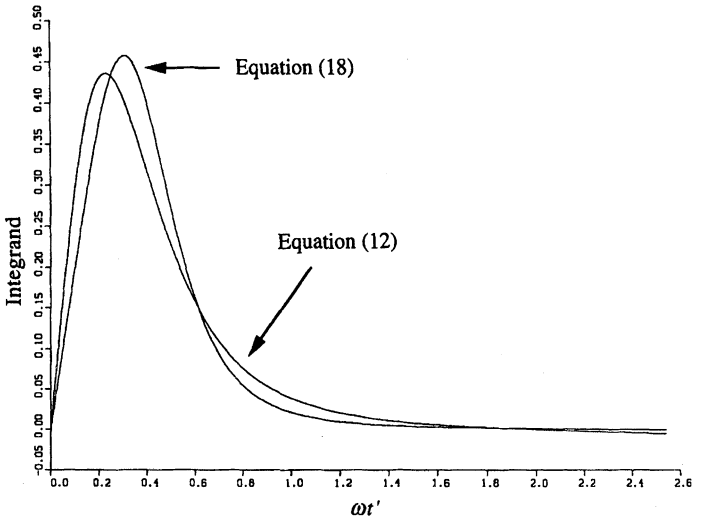

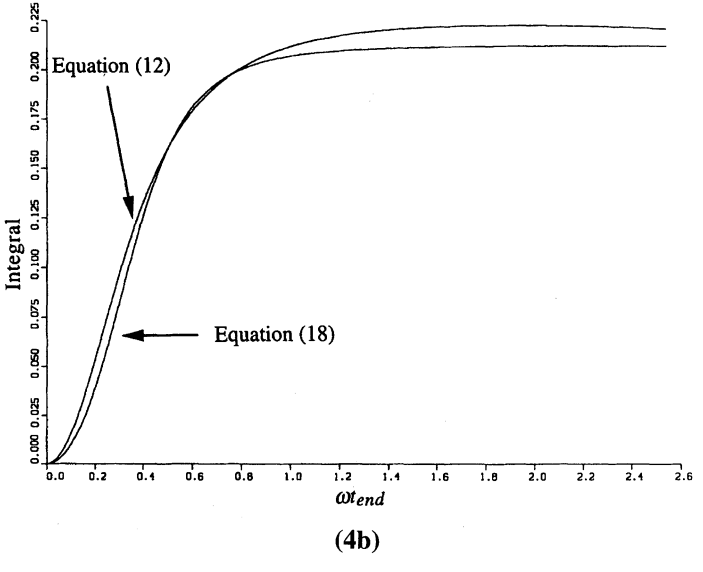

FIGURE 4 Comparison of Equations (12) and (18) for $\alpha = 2$ and $\phi_o = 0.6$. (a) Comparison of the integrands as functions of $\omega t'$. (b) Comparison of the integrals as functions of t_{end}.

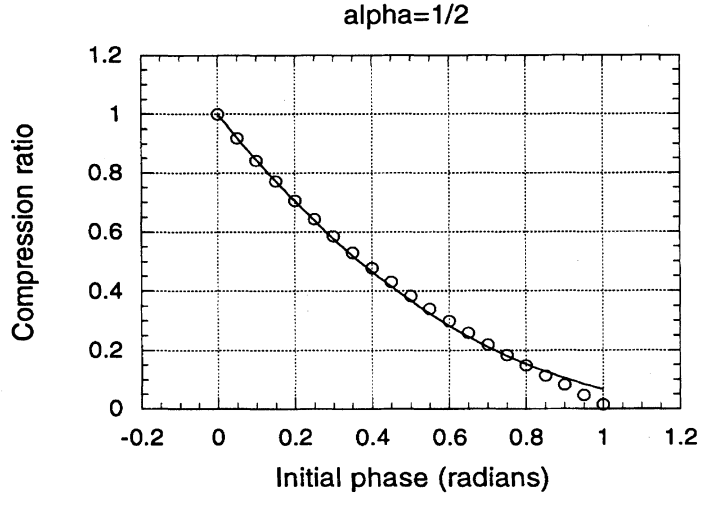

(5a)

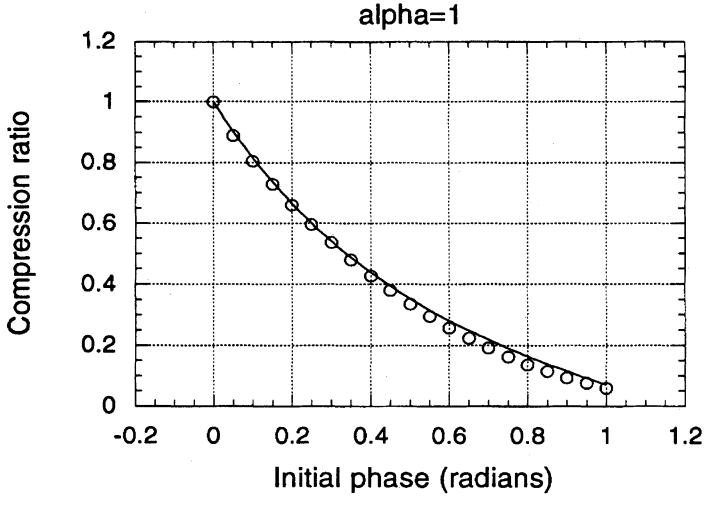

(5b)

FIGURE 5 Compression ratio versus rf start phase. The solid lines are from the integral given by Equation (12) and the circles are the solutions of the approximate fit described by Equation (20), (a) $\alpha = \frac{1}{2}$, (b) $\alpha = 1$, (c) $\alpha = 2$.

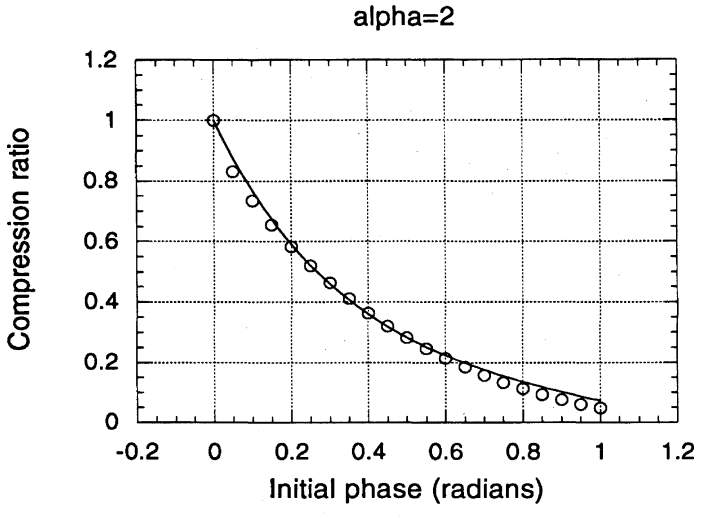

(5c)

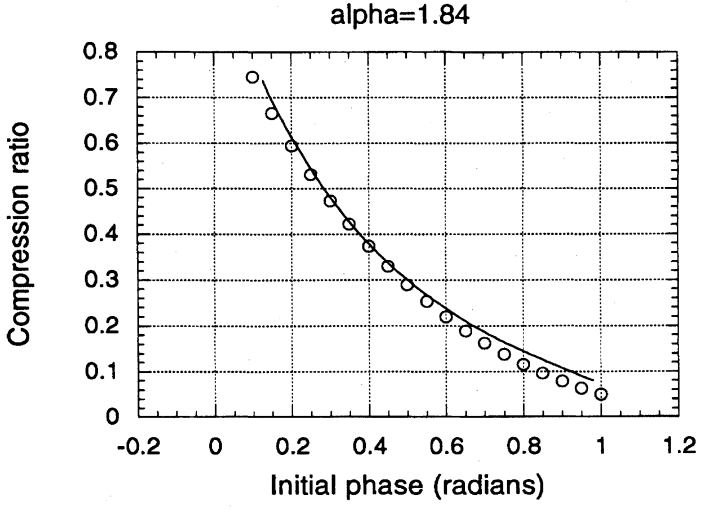

FIGURE 6 Compression ratio versus rf start phase for $\alpha = 1.84$. The solid line is generated by PARMELA simulations for the Brookhaven photoinjector and the circles are the solutions of the approximate fit described by Equation (20).

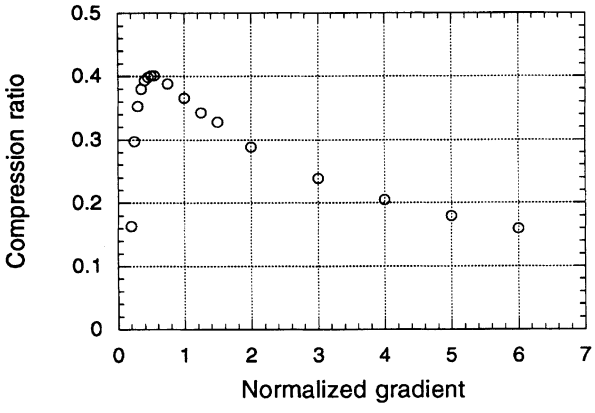

FIGURE 7 Compression ratio versus normalized gradient α for a 0.5 radian start phase. The circles were generated by PARMELA simulations for the Brookhaven photoinjector and should be compared to Figure 2.

we would have predicted a peak field of about 118 MV/m on the cathode; this slight deviation is due to geometry effects in the cavity leading to the presence of higher-order space harmonics.) The assumed bunch in the PARMELA simulations was initially 1-ps long, with a very small radius (100 μm) and negligible charge. The agreement is very good. Additionally, the PARMELA simulations indicated that for this case, the compressed rms bunch length increased less than 50 fs (added in quadrature) per millimeter of bunch radius, due to the radial nonuniformity in the axial electric rf field.

In Figure 7 we plot the compression ratio calculated by PARMELA for this photoinjector versus normalized gradient, for an initial rf phase of 0.5 radian. The results are nearly identical to those plotted in Figure 2, which were found from solving Equations (1)–(3) and (12) (recall that the points along the branch with the short dashes in Figure 2 were for a constant length cavity). The bunch actually expands for some normalized gradients less than about 0.15.

7 FINAL BUNCH LENGTH INCLUDING SPACE CHARGE

Using Equation (20) above and the treatment of space charge in Reference 9, we can write the following expression for the final bunch length of a short

bunch with initial phase duration $\Delta\phi_o$:

$$\frac{\Delta l}{\beta c} = \frac{\Delta\phi_o}{\omega} - \frac{\Delta\phi_o}{\beta\omega\sqrt{\alpha^{*2}(1+\cos\phi_o)^2+1}} \frac{4\alpha(1-\sin\phi_o)\cos\phi_o}{1+2\phi_o/\pi} + \frac{16Qc^3}{I_A\alpha^2\omega^2R^2\sin^2\phi}\log(2) \tag{21}$$

where Q is the bunch charge, I_A is the Alfven current, R is the beam radius at the cathode, and ϕ is the asymptotic phase of the bunch center. This expression is valid only if the bunch is short both in the regard that the second order compression ratio is not important and also that the bunch is short in its rest frame relative to its radius ($\Delta\phi_o c/\omega \ll R$). Note that the initial bunch length does not appear in the expression for the space-charge induced expansion, because near the cathode the bunch length is very much smaller than the bunch radius.

8 CONCLUSION

We have shown that a simple modification to the form of the axial electric field leads to an integral expression for the longitudinal contraction of an electron bunch due to rf forces in a photoinjector. We have numerically shown that this integral expression agrees very well with the exact solution, found by numerically pushing particles in the first cavity of an rf photoinjector. We have found an approximate solution to the integral in the region of gradients corresponding to existing and planned photoinjectors (which is valid to a few percent in the amount of compression). In addition, we have shown that this approximate solution agrees very well with detailed numerical simulations of an existing photoinjector. We have also seen that compressions larger than 50% of the drive laser pulse length are possible for start phases below 0.5 radian. In practice, these results imply that for maximum rf compression the normalized gradient in the photoinjector should be in the range of $1/2-1$.

References

[1] Dei-Cas, R., Balleyguier, P., Beuve, M.A., Binet, A., Bleses, J.P., Bloquet, A., Bois, R., Bonetti, Cl., Brisset, J., De Brion, J.P., Di Crescenzo, J., Dolique, J.M., Faujour, R., Fourdin, P., Frehaut, J., Guilloud, M., Haouat, G., Iracane, D., Joly, R., Joly, S., Laget,

J.P., Laspalles, Cl., Leboutet, H., Marmouget, J.G., Masseron, D., Michaud, P., Pranal, Y., Seguin, S., Striby, S., Schumann, F. and Vouillarmet, J. (1992). "Photoemission studies and commissioning the ELSA-FEL experiment", *Nucl. Instrum. Meth. Phys. Res.*, **A318**, 121.

[2] Dowell, D.H. *et al.* (1993). "First operation of a photocathode radio frequency gun injector at high duty factor", *Appl. Phys. Lett.*, **63**(15).

[3] O'Shea, P.G., Bender, S.C., Carlsten, B.E., Early, J.W., Feldman, D.W., Lumpkin, A.H., Feldman, R.B., Goldstein, J.C., McKenna, K.F., Martineau, R., Pitcher, E.J., Schmitt, M.J., Stein, W.E., Wilke, M.D. and Zaugg, T.J. (1993). "Performance of the APEX free-electron laser at Los Alamos National Laboratory", *Nucl. Instrum. Meth. Phys. Res.*, **A331**, 62.

[4] Sheffield, R.L., Austin, R.H., Chan, K.D.C., Gierman, S.M., Kinross-Wright, J.M., Kong, S.H., Nguyen, D.C., Russell, S.J. and Timmer, C.A. (1993). "Operation of the high-brightness linac for the advanced free-electron laser initiative at Los Alamos", *Proceedings of the 1993 IEEE Particle Accelerator Conference*, **IEEE 93CH3279-7**, 2970.

[5] Wang, X.J., Babzien, M., Batchelor, K., Ben-Zvi, I., Malone, R., Pogorelsky, I., Qui, X., Sheehan, J., Skaritka, J. and Srinivasan-Rao, T., "Experimental characterization of high-brightness electron photoinjector", submitted to *Phys. Rev. Lett.*

[6] Chen, S.C., Gonichon, J., Lin, L.C-L., Temkin, R.J., Trotz, S., Danly, B.G. and Wurtele, J.S. (1993). "High gradient acceleration in a 17 GHz photocathode rf gun", *Proceedings of the 1993 IEEE Particle Accelerator Conference*, **IEEE 93CH3279-7**, 2575.

[7] Pelligrini, C. (1995). Private communication.

[8] Katsouleas, T. (1995). Private communication.

[9] Serafini, L. (1996). "Micro-bunch production with radio frequency photoinjectors", *IEEE Trans. Plas. Sci.*, **24**, 421.

[10] Young, L. (1989). Private communication.

[11] Kim, K.J. (1989). "RF and space-charge effects in laser-driven rf electron guns", *Nucl. Instrum. Meth. Phys. Res.*, **A275**, 201.

[12] Chen, S.C. (1993). "High gradient acceleration in a 17 GHz photocathode rf gun", *AIP Conf. Proc.*, **279**, 694.

[13] Wang, X. (1992). "High-brightness electron accelerator injection system and experimental studies of laser-induced explosive electron emission", PhD Thesis, University of California, Los Angeles, UCLA-CAA0086-2/92.

[14] Wang, X.J., Qiu, X. and Ben-Zvi, I., "Experimental observation of micro-bunching in a photocathode rf gun injector", submitted to *Phys. Rev. Lett.*

[15] Serafini, L. (1995). "Analytic description of particle motion in radio-frequency photoinjectors", *Particle Accelerators*, **49**, 253.

[16] Young, L. (1995). Private communication.